AGU PUBLICATIONS

Paleoceanography

RESEARCH ARTICLE
10.1002/2015PA002818

Key Points:
- We test hypothesized drivers of the carbon cycle perturbation at the Eocene-Oligocene transition
- Only reduced shelf carbonate burial and a carbonate weathering pulse can explain the CCD deepening
- Permafrost or peat expansion can help explain the rapid carbon isotope excursion steps

Supporting Information:
- Texts S1 and S2, Figures S1–S3, and Tables S1–S3

Correspondence to:
D. I. Armstrong McKay,
D.Armstrong-McKay@noc.soton.ac.uk

Citation:
Armstrong McKay, D. I., T. Tyrrell, and P. A. Wilson (2016), Global carbon cycle perturbation across the Eocene-Oligocene climate transition, *Paleoceanography*, *31*, 311–329, doi:10.1002/2015PA002818.

Received 24 APR 2015
Accepted 19 JAN 2016
Accepted article online 22 JAN 2016
Published online 20 FEB 2016

Global carbon cycle perturbation across the Eocene-Oligocene climate transition

David I. Armstrong McKay[1,2], Toby Tyrrell[1], and Paul A. Wilson[1]

[1]National Oceanography Centre, Southampton, University of Southampton, Southampton, UK, [2]Geography and Environment, University of Southampton, Southampton, UK

Abstract The Eocene-Oligocene transition (EOT), ~34 Ma, marks a tipping point in the long-term Cenozoic greenhouse to icehouse climate transition. Paleorecords reveal stepwise rapid cooling and ice growth across the EOT tightly coupled to a transient benthic $\delta^{13}C$ excursion and a major and permanent deepening of the carbonate compensation depth (CCD). Based on biogeochemical box modeling, Merico et al. (2008) suggested that a combination of (1) glacioeustatic sea level fall-induced shelf-basin carbonate burial fractionation and (2) shelf carbonate weathering can account for the carbon cycle perturbation, but this finding has been questioned. Alternative proposed mechanisms include increased ocean ventilation, decreased carbonate burial, increased organic carbon burial, increased silicate weathering, and increased ocean calcium concentration. Here we use an improved version of the biogeochemical box model of Merico et al. (2008) to reevaluate these competing hypotheses and an additional mechanism, the expansion of "carbon capacitors" such as permafrost and peatlands. We find that changes in calcium concentration, silicate weathering, and carbonate or organic carbon burial each yield a response that is fundamentally at odds with the form and/or sign of the paleorecords. Shelf-basin carbonate burial fractionation (CCD change), plus shelf carbonate weathering, sequestration of ^{12}C-enriched carbon into carbon capacitors, and possibly increased ocean ventilation ($\delta^{13}C$ excursion), offers the best fit to the paleorecords. Further work is needed to understand why the EOT carbon cycle perturbation is so unique when the forcing mechanisms hypothesized to be responsible (cooling and ice growth) are not peculiar to this event.

1. Background

1.1. The Eocene-Oligocene Transition

The first permanent, large-scale ice sheets on Antarctica were established during the Eocene-Oligocene transition (EOT) ~34 Ma, the point at which Earth's climate transitioned from a late Cretaceous-early Paleogene greenhouse state to a late Paleogene-Neogene icehouse state [*Zachos et al.*, 2001]. Paleorecords of high-latitude climate change (benthic $\delta^{18}O$) reveal stepwise cooling and ice sheet growth at ~34.0 Ma (EOT-1) and ~33.7 Ma (Oi-1) (Figure 1a) [*Coxall et al.*, 2005; *Coxall and Wilson*, 2011], with a cooling of between 2 and 6°C mostly during the first step and ice sheet growth equivalent to 60 to 130% of modern Antarctic ice volume mostly during the second step [*Coxall et al.*, 2005; *Lear et al.*, 2008; *Miller et al.*, 2008; *Liu et al.*, 2009; *Scher et al.*, 2011; *Tigchelaar et al.*, 2011; *Wade et al.*, 2011; *Bohaty et al.*, 2012]. These steps are accompanied by an ~1.0‰ $\delta^{13}C$ excursion in benthic foraminifera, peaking between 34.0 and 33.7 Ma and followed by a decline to ~0.1‰ above late Eocene values by ~32.5 Ma (Figure 1b), along with a deepening of the carbonate compensation depth (CCD), initially by around 1200 m but by around 500 m in the long term (Figure 1c), suggesting a strong coupling between this climatic shift and the carbon cycle [*Coxall et al.*, 2005; *Rea and Lyle*, 2005; *Coxall and Wilson*, 2011; *Pälike et al.*, 2012]. The $\delta^{18}O$ records take a form similar to that indicated by the results of coupled global climate-ice sheet model experiments [*DeConto and Pollard*, 2003; *Ladant et al.*, 2014] in which a slow decline of atmospheric CO_2 ($_{atm}CO_2$) (Figure 1d) [*Pearson et al.*, 2009; *Pagani et al.*, 2011; *Heureux and Rickaby*, 2015] and superimposed orbital forcing bring about the crossing of a critical threshold for the initiation of rapid Antarctic glaciation.

1.2. Potential Drivers of the EOT Carbon Cycle Perturbation

1.2.1. Carbonate Burial and Weathering

Merico et al. [2008] used a biogeochemical box model to test several mechanisms proposed in the contemporary literature for the EOT carbon cycle perturbation, including increases in organic carbon (C_{org}) burial rates, global silicate weathering rates, and siliceous plankton productivity. However, these

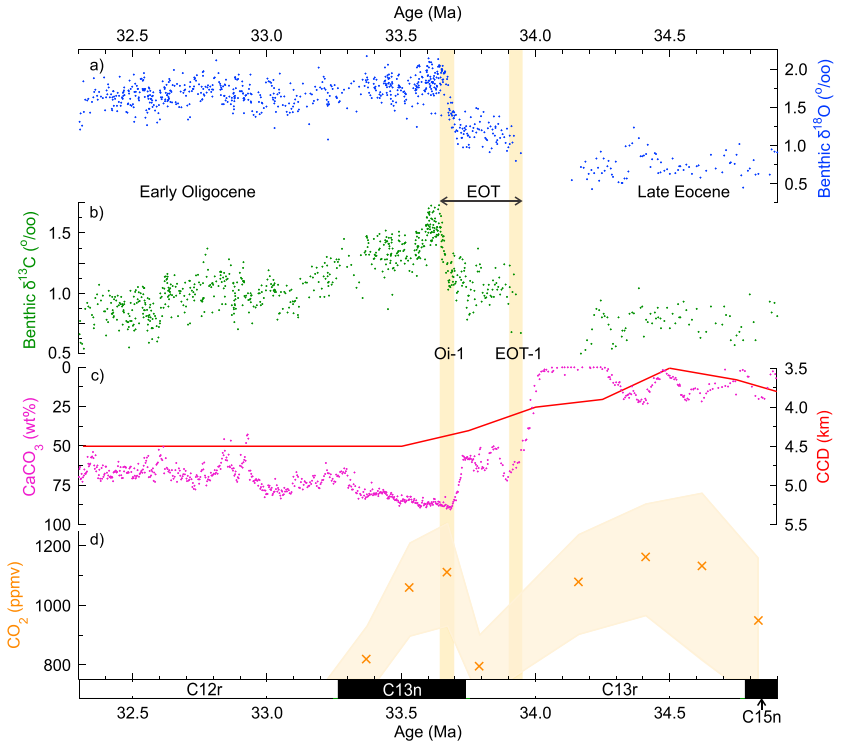

Figure 1. Paleorecords across the Eocene-Oligocene transition (EOT). (a) Benthic $\delta^{18}O$ from ODP Site 1218 (8°53′N, 135°22′W in the equatorial Pacific) (blue) [*Coxall and Wilson*, 2011], (b) benthic $\delta^{13}C$ from ODP Site 1218 (green) [*Coxall and Wilson*, 2011], (c) the long-term behavior of the CCD in the equatorial Pacific (red line) [*Pälike et al.*, 2012] and $CaCO_3$ wt % from IODP Site 1218 as a qualitative proxy for CCD deepening in the equatorial Pacific (purple dots) [*Coxall et al.*, 2005; *Coxall and Wilson*, 2011] (using the age model of *Westerhold et al.* [2014]), and (d) $_{atm}CO_2$ reconstructed from the boron isotope pH proxy (orange crosses, shaded band for uncertainty) [*Pearson et al.*, 2009] between the late Eocene and the early Oligocene. The EOT-1 and Oi-1 cooling and glaciation steps are indicated by the yellow bars, and the Geomagnetic Polarity Timescale [*Ogg and Smith*, 2004] is shown along the bottom axis.

hypotheses were ultimately rejected on the basis of failing to simultaneously match both the permanent CCD deepening and the temporary positive benthic $\delta^{13}C$ excursion observed in the paleorecord. The only hypothesis found to replicate successfully these two simulation targets was a shift in $CaCO_3$ burial from shallow shelf seas to the deep ocean coupled with a temporary increase in carbonate weathering from freshly exposed, fast-weathering, and ^{13}C-enriched carbonate shelves. These changes were hypothesized to be driven by the 50 to 75 m fall in sea level associated with the growth of the Antarctic ice sheet [*Pekar et al.*, 2002; *Lear et al.*, 2004; *Miller et al.*, 2008; *de Boer et al.*, 2010; *Houben et al.*, 2012]. In this explanation of events the fall in sea level reduces the area of shallow shelf seas available for carbonate burial, which results in an increase in the calcite (and aragonite) saturation state (Ω) of the ocean and consequently a deepening of the CCD until the increase in deep-ocean carbonate burial compensates for the reduction in shelf burial, a scenario supported by observations of a major shift in carbonate burial from shelf to basin settings from the Eocene to Oligocene [*Berger and Winterer*, 1975; *Opdyke and Wilkinson*, 1988; *Kump and Arthur*, 1997; *Coxall et al.*, 2005; *Lear and Rosenthal*, 2006; *Merico et al.*, 2008]. Proxies suggest that the establishment of the Antarctic ice sheet temporarily led to increased glacial erosion facilitating greater chemical weatherability in Antarctica which, along with the exposure of large areas of highly weatherable shelf carbonates, led to temporarily heightened carbonate weatherability and in turn global carbonate weathering rates [*Zachos et al.*, 1999; *Ravizza and Peucker-Ehrenbrink*, 2003; *Griffith et al.*, 2011; *Scher et al.*, 2011; *Basak and Martin*, 2013; *Moore*, 2013]. However, this hypothesis requires a big shift in carbonate burial from shallow to deep water (~99% in *Merico et al.* [2008]) and a substantial increase in carbonate weathering (300% in *Merico et al.* [2008]) to match fully the amplitude of change in the paleorecords. Critiques of this hypothesis suggest that the sea level fall across the EOT is

insufficiently large and unique to cause such a large and permanent change in both shelf carbonate burial and weathering [*Rea and Lyle*, 2005; *Miller et al*., 2009].

1.2.2. Ventilation and Productivity

Increased ocean mixing rates across the EOT are a likely response to high-latitude cooling and ice sheet growth [*Zachos et al*., 1996; *Goldner et al*., 2014]. It has been hypothesized that increased ocean mixing ventilated the deep ocean and reduced deep-ocean acidity sufficiently to deepen the CCD [*Miller et al*., 2009]. Increased mixing has also been invoked as a means of stimulating plankton productivity, particularly diatom productivity in the Southern Ocean, by upwelling nutrients from deep water, which results in a positive benthic $\delta^{13}C$ perturbation due to elevated C_{org} export and burial relative to carbonate (i.e., a decrease in the $CaCO_3$:C_{org} rain ratio) [*Salamy and Zachos*, 1999; *Zachos and Kump*, 2005; *Scher and Martin*, 2006; *Berger*, 2007; *Dunkley Jones et al*., 2008; *Scher et al*., 2011]. An increase in C_{org} burial can also be achieved through an increase in C_{org} preservation, for example, through a shift in production to upwelling zones with high sedimentation rates or due to cooler deep water from greater polar deepwater formation [*Zachos et al*., 1996; *Olivarez Lyle and Lyle*, 2006; *John et al*., 2014]. All of these hypotheses were tested by *Merico et al*. [2008], but their efficacy was called into question. The results of those experiments indicated that ocean mixing and productivity should be ruled out as sole drivers of the observed carbon cycle perturbation because both mechanisms produce a permanent rather than a temporary benthic $\delta^{13}C$ excursion and a temporary rather than a permanent CCD deepening. Furthermore, the observations of *Griffith et al*. [2010] cast doubt on the likelihood of there having been a significant increase in C_{org} export across the EOT. An increase in C_{org} export and burial relative to carbonate would, all else remaining equal, be expected to lead to a decrease in the global $CaCO_3$:C_{org} surface export ratio (known as the rain ratio), but increased $CaCO_3$ accumulation relative to barite accumulation across the EOT instead points to relatively minor changes in C_{org} burial relative to $CaCO_3$ export, suggesting an overall increase in the rain ratio.

1.2.3. Silicate Weathering and Calcium

Another hypothesized driver of the EOT CCD deepening is an increase in the input of calcium ion (Ca^{2+}) to the ocean through increased silicate weathering which raises ocean Ω [*Rea and Lyle*, 2005; *Lyle et al*., 2008]. Increased silicate weathering, in response to increased Antarctic weatherability, has also been invoked as a source of additional alkalinity input to the ocean, helping to deepen the CCD and to provide a positive feedback on glaciation through the drawdown of $_{atm}CO_2$ [*Zachos and Kump*, 2005; *Griffith et al*., 2011; *Scher et al*., 2011; *van de Flierdt*, 2011; *Basak and Martin*, 2013]. Ca^{2+} input to the ocean is primarily derived from continental weathering and oceanic hydrothermal systems. Continental weathering acts to increase ocean Ω through delivery of Ca^{2+} and HCO_3^- which results in the deepening of the CCD and increased Ca^{2+} removal through burial [*Farkaš et al*., 2007b; *Komar and Zeebe*, 2011]. To exert any significant impact on oceanic Ca^{2+} concentration ($[Ca^{2+}]$), therefore, it is necessary to decouple the input of Ca^{2+} from bicarbonate input. This is possible through increased dolomitization, hydrothermal Ca^{2+} input, or sulfuric-acid-driven weathering [*Heuser et al*., 2005; *Farkaš et al*., 2007a], but a large change in Ca^{2+} delivery is required to overcome the long (~1 Myr) residence time of Ca^{2+} in the ocean. Paleorecords of $\delta^{44/40}Ca$ in bulk marine carbonates across the EOT show a negative excursion in bulk carbonate of ~0.6‰ which has been attributed to increased Ca^{2+} flux to the ocean as a result of an increase in silicate weathering [*De La Rocha*, 2000; *Fantle*, 2010]. However, $\delta^{44/40}Ca$ records generated across the EOT on marine barites, suggested to be a more reliable record of calcium isotope changes, yield a smaller shift in reconstructed seawater $\delta^{44/40}Ca$, suggesting little change in silicate weathering and/or Ca^{2+} delivery to the ocean across the EOT [*Griffith et al*., 2011].

1.2.4. Carbon Capacitors and Cooling

Other potential drivers of carbon cycle disruptions across the EOT involve various reservoirs of sedimentary C_{org} capable of rapid exchange with the ocean-atmosphere system. These include carbon stored in permafrost, marine methane hydrates, peat, wetlands, and soil. Permafrost soil carbon (PFSC) deposits in the Northern Hemisphere (NH) today contain up to ~1700 Pg of carbon [*Tarnocai et al*., 2009; *Koven et al*., 2011], but modeling suggests that the late Eocene inventory was more than double this present-day figure (~3700 Pg C: ~2000 Pg C in NH; ~1700 Pg C in Antarctica) because of expanded wetlands and peatlands in a greenhouse climate [*DeConto et al*., 2012]. This estimated inventory for the Eocene is even bigger than that estimated for the last glacial when approximately 2700 Pg C is estimated to have been sequestered by expanded NH permafrost regions [*Zimov et al*., 2009; *Zech et al*., 2011]. Modern peatlands are estimated to contain between 180 and 455 Pg C of a total global soil inventory of ~2400 Pg C, and this reservoir is

hypothesized to have sequestered a further ~ 500 Pg C during the Last Glacial Maximum [*Klinger*, 1991; *Batjes*, 1996; *Klinger et al*., 1996; *MacDonald et al*., 2006]. Methane hydrates in marine sediments are estimated to contain between 450 and 3000 Pg C today and are hypothesized to have had a similar inventory in the Eocene [*Buffett and Archer*, 2004; *Dickens*, 2011; *Wallmann et al*., 2012], although the total inventory is uncertain even in the modern. Together, these three reservoirs contain a substantial inventory of carbon, and changes to their storage capacity are capable of rapidly perturbing the exogenic carbon cycle.

We might expect the storage capacity of these "carbon capacitors" [*Dickens*, 2011] to have grown during the EOT because of global and particularly high-latitude cooling. In fact, the growth and subsequent decline of methane hydrate reservoirs has been invoked as a potential driver of the EOT $\delta^{13}C$ excursion [*Berger*, 2007]. Arctic PFSC is modeled to expand by ~1300 Pg as $_{atm}CO_2$ falls from 900 to 550 ppmv [*DeConto et al*., 2012], and a simulation of modern PFSC indicates that permafrost processes enhance carbon sequestration [*Koven et al*., 2011], potentially acting as a positive feedback on cooling. We might also expect CO_2 drawdown through these mechanisms to have been opposed by CO_2 release through the erosive action of advancing ice sheets on Antarctic permafrost. Yet recent discoveries of preglacial soils preserved beneath the Greenland Ice Sheet and methanogenesis continuing in sub-Antarctic sediments indicate that a significant proportion of PFSC can survive the growth of ice sheets [*Wadham et al*., 2012; *Bierman et al*., 2014], and PFSC sequestration below ice sheets has been invoked as part of the glacial burial hypothesis of Pleistocene $_{atm}CO_2$ variability [*Zeng*, 2003]. If a significant proportion of Antarctic PFSC was sequestered below advancing ice sheets or in sediments, then expansion of PFSC or other C_{org} reservoirs elsewhere in response to global cooling could have resulted in a net positive $\delta^{13}C$ excursion and a drawdown of $_{atm}CO_2$ across the EOT.

1.3. Study Aims

To test each of the competing hypothesized mechanisms responsible for the EOT carbon cycle perturbation, we undertake biogeochemical box model simulations of each hypothesis to determine the changes necessary to match the geochemical excursions observed in the paleorecord. We then evaluate whether these changes are feasible within the constraints of the late Eocene Earth system.

2. Method

2.1. Modeling

We use an improved version of the biogeochemical box model of *Merico et al*. [2008] (hereafter referred to as MTW08) to explore new hypotheses not considered in *Merico et al*. [2008] and to reexamine longer-standing hypotheses in more detail. MTW08 is an open system containing all the major fluxes and processes in the carbon, phosphorus, and silicon cycles, including the carbonate system, air-sea gas exchange, the organic matter pump, $_{atm}CO_2$ drawdown by silicate weathering, calcium carbonate formation and cycling, and carbon isotopes (model schematic shown in supporting information Figure S1). For this study we have also added the impact of dynamic changes in the ocean $[Mg^{2+}]/[Ca^{2+}]$ ratio on ocean Ω to the model to capture better the impact of hypothesized changes in $[Ca^{2+}]$ during the EOT. To do this, we incorporate the estimated impact of the $[Mg^{2+}]/[Ca^{2+}]$ ratio on the stoichiometric solubility product of calcite and aragonite and the dissociation constants of carbonic acid [*Ben-Yaakov and Goldhaber*, 1973; *Mucci and Morse*, 1984; *Tyrrell and Zeebe*, 2004]. More advanced formulations of the impact of $[Mg^{2+}]/[Ca^{2+}]$ on carbonate chemistry have recently been developed [*Hain et al*., 2015], but this formulation has not yet been included into MTW08. MTW08 remains limited by low spatial resolution, uncertainties in late Eocene estimates for model parameters, and the lack of dynamic ocean-atmosphere circulation, terrestrial biosphere, or ocean sediment components. MTW08 parameters were tuned with estimates for late Eocene conditions (supporting information Tables S1 and S2) and perturbed by various different scenarios for each of the hypotheses outlined in section 2.2.

First, in a set of conceptual simulations, we test each hypothesized mechanism in isolation to illustrate its impact on $\delta^{13}C$, the CCD, and $_{atm}CO_2$ (Figure 2). Then we test different combinations of hypotheses as described in section 2.2 (Figures 3–8). Our simulation targets are as follows: (1) a permanent, 500 m deepening of the CCD with an initial stepwise overdeepening of up to ~1200 m and (2) a $>+0.7‰$ benthic $\delta^{13}C$ excursion over ~1 Myr with rapid increases at EOT-1 and Oi-1 peaking at a maximum of ~ +1.0‰ at Oi-1.

Both targets feature strong steps at EOT-1 and Oi-1 with the latter being larger, and so we partition the proposed mechanisms between both steps (in most cases by one-third at EOT-1 and two-thirds at Oi-1). We do not use $_{atm}CO_2$ as a simulation target because of the limitations of the paleorecords available, but our model results for $_{atm}CO_2$ are shown and discussed. We compare our model results with the benthic $\delta^{13}C$, CCD, and $_{atm}CO_2$ paleorecords plotted in Figure 1. Our long-term CCD target is based on the reconstruction of *Pälike et al*. [2012] from equatorial sites in the world's biggest basin, the Pacific Ocean, which we assume to be broadly globally representative. Note that we use $CaCO_3$ wt % as a qualitative proxy of the timing (but not amplitude) of CCD stepwise overdeepening because the widely observed overdeepening is not resolved by the reconstruction of *Pälike et al*. [2012]. The amplitude of the initial CCD deepening is estimated at ≤1200 m [*Rea and Lyle*, 2005]. Previous analyses of the sensitivity of MTW08 to parameter selection have demonstrated that the results of MTW08 simulations are relatively robust to parameter choices [*Merico et al*., 2008; *Armstrong McKay et al*., 2014]. We also quantify the model-data fit for $\delta^{13}C$, by calculating the root mean square error (RMSE) between the filtered data and the model results, but not for the CCD or $_{atm}CO_2$ due to limited data quality (see supporting information Text S1).

2.2. Hypotheses

In this section we define and summarize five main hypotheses to test and then describe how each of these hypotheses is simulated in this study. These hypotheses are based on our assessment of the literature on the proposed drivers of the EOT carbon cycle perturbation (see section 1.2).

2.2.1. Carbonate Burial Fractionation

In this hypothesis a glacioeustatic fall in sea level results in a decrease in shelf carbonate burial and, through carbonate compensation, an increase in ocean Ω to compensate and a deepening of the CCD until ocean Ω stabilizes. It also includes additional carbonate weathering because of the rapid weathering of formerly submerged carbonate shelves, which we simulate as more enriched in ^{13}C than pelagic carbonate ($\delta^{13}C$ of 1.5‰ versus 0.28‰ in the Eocene MTW08 tuning, based on paleorecords and modern observations from Great Bahama Bank which are enriched by ~4.8‰ relative to pelagic carbonate [*Swart and Eberli*, 2005; *Merico et al*., 2008; *Swart*, 2008; *Swart et al*., 2009; *Oehlert et al*., 2012]) and so can contribute to a positive benthic $\delta^{13}C$ excursion. To simulate this hypothesis, we (1) reduce the proportion of carbonate burial in shallow settings (from the model baseline of ~45%; a very conservative estimate for the shelf carbonate burial-rich Eocene [*Opdyke and Wilkinson*, 1988] but the same as *Merico et al*. [2008] to allow direct comparison) and (2) add an extra source of carbonate weathering separate to the baseline global weathering rate in order to represent a weathering pulse from highly weatherable newly exposed subaerial shelf carbonates.

In some runs a simultaneous increase in weathering of C_{org} and silicate-rich lithologies and an increase in riverine nutrient input to the ocean are also simulated to represent the weathering of noncarbonate components of exposed shelves [*Scher et al*., 2011]. Some estimates of weathering rate differences between the Holocene and the Last Glacial Maximum (LGM) suggest that although total weathering rates were only marginally higher at the LGM, carbonate weathering was enhanced relative to silicate weathering in response to glaciation (attributable to a greater prevalence of carbonates with high weatherability on exposed low-latitude shelves versus the land area covered by ice sheets) [*Gibbs and Kump*, 1994; *Munhoven*, 2002]. Based on this pattern and the even greater prevalence of shelf carbonate platforms in the Eocene [*Opdyke and Wilkinson*, 1988], we assume that carbonate weathering would increase by a greater magnitude even if the weathering of C_{org}-rich and silicate lithologies was also enhanced at the EOT.

2.2.2. Increased Ocean Ventilation

In this hypothesis an increase in ocean ventilation results in a reduction in deep-ocean acidity and thus deepens the CCD. It also stimulates (at least for a time) an increase in productivity through the upwelling of deepwater nutrients, which is predicted to drive an increase in ocean $\delta^{13}C$. To simulate this hypothesis, we take the same approach as *Merico et al*. [2008] and increase the surface-to-middle and the middle-to-deep ocean mixing rates (from the Eocene MTW08 baseline ocean mixing coefficients of 18.25 and 3.0 my^{-1}, respectively [*Broecker and Peng*, 1982; *Chuck et al*., 2005]) in two steps at EOT-1 and Oi-1 by varying proportions. This increase is simulated both as a permanent change and as temporary increases during EOT-1 and Oi-1 in response to glaciation-induced intensification of ocean overturning, returning to baseline by 33.0 Ma. It is unlikely, however, that EOT cooling produced a permanent increase in mixing rates because once ocean

temperature gradients stabilize then global-scale vertical mixing in the ocean is expected to gradually return to pre-perturbation rates. It should also be noted that although there is evidence of increased ocean mixing in the Southern Ocean at the EOT [*Kennett and Shackleton*, 1976; *Kennett*, 1977; *Salamy and Zachos*, 1999], the absolute increase in global ocean mixing rates has not been constrained.

2.2.3. Carbon Capacitor Exchange

In this hypothesis, not considered by *Merico et al.* [2008], cooling across the EOT results in net expansion of carbon capacitors such as PFSC in the Northern Hemisphere and therefore a positive benthic $\delta^{13}C$ excursion through oceanic depletion in ^{12}C. Although methane hydrates have been proposed as a potential ^{12}C-rich sink during the EOT [*Berger*, 2007], the impact of changing sea level and continental shelf loss complicates the likely response of this reservoir at the EOT. We therefore focus on the potential reaction of two related carbon capacitors, the PFSC and peatland ^{12}C-rich reservoirs. To simulate this hypothesis, we directly remove carbon (with $\delta^{13}C$ of $-23‰$) from the atmosphere during both Oi-1 and EOT-1. A sink that sequesters more ^{12}C-enriched carbon such as marine hydrate requires a commensurately smaller flux. There is relatively little information available to constrain the likely magnitude and timing of PFSC drawdown, but simulations of PFSC release and expansion during the early Eocene suggest that several thousand petagrams of PFSC can form within 1 to 10 kyr [*DeConto et al.*, 2012]. We hypothesize that up to a similar-sized expansion in the PFSC reservoir could take place during each of the two ~40 kyr long EOT steps. To simulate the counterhypothesis of net PFSC erosion rather than uptake, we instead add carbon with the same isotopic composition to the atmosphere.

2.2.4. Export and Burial Flux Changes

In this hypothesis either a decrease in $CaCO_3$ export and burial relative to C_{org} or an increase in C_{org} burial driven by increasing C_{org} preservation in seafloor sediments results in the positive benthic $\delta^{13}C$ excursion through decreased ^{13}C or increased ^{12}C removal from the ocean. A reduction in $CaCO_3$ burial should also deepen the CCD to compensate for rising $[CO_3^{2-}]$, while increasing C_{org} preservation reduces the concentration of deep-ocean dissolved inorganic carbon (DIC). To simulate these hypotheses, we perform two different experiments. In one we reduce the rain ratio (from the Eocene MTW08 baseline ratio of 0.298) resulting in reduced $CaCO_3$ export. In the second we increase the proportion of organic carbon buried in sediment (from the Eocene MTW08 baseline of ~0.1%) which in turn also decreases the proportion of carbon remineralized in the deep ocean. The changes in both experiments occur during two steps at EOT-1 and Oi-1, and various magnitudes of change are tested.

2.2.5. Increased Silicate Weathering and Calcium Flux to the Ocean

In this hypothesis increasing concentrations of Ca^{2+} and/or alkalinity in the ocean, attributable to either an increase in silicate weathering or a direct increase in Ca^{2+} input decoupled from weathering, results in an increase in ocean Ω and therefore a deepening of the CCD while also drawing down $_{atm}CO_2$ and therefore acting as a positive feedback on glaciation. To simulate this hypothesis, we undertake two different experiments. In the first we simulate an increase in silicate weathering attributable to elevated weatherability by adding an extra source of silicate weathering separate from the baseline global weathering rate to deliver an increased supply of both Ca^{2+} and alkalinity to the ocean, a similar experiment to one in *Merico et al.* [2008]. In the second we directly increase the input of Ca^{2+} to the ocean without also increasing weathering in order to isolate the influence of Ca^{2+} addition, a scenario not tested by *Merico et al.* [2008].

3. Results and Discussion

3.1. Scenarios

3.1.1. Carbonate Burial Fractionation

Figures 2 and 3 illustrate the results of varying the magnitudes of shelf carbonate burial and/or weathering by differing amounts. We first replicate the favored scenario of *Merico et al.* [2008] by (1) adding a temporary 300% stepped increase (100% step at EOT-1) in carbonate weathering separately to the baseline global weathering rate to represent the newly exposed highly weatherable shelf source (increased weatherability) by the time of Oi-1 to match the benthic $\delta^{13}C$ excursion and (2) permanently reducing the proportion of carbonate buried on shelves by 99% at EOT-1 to permanently deepen the CCD by ~600 m. However, the magnitude of additional carbonate weathering required to fully match the benthic $\delta^{13}C$ excursion produces an initial CCD overdeepening of ~2000 m compared to the target of $\leq$1200 m, indicating that such a large increase in carbonate weathering is excessive if the records from the equatorial Pacific are globally

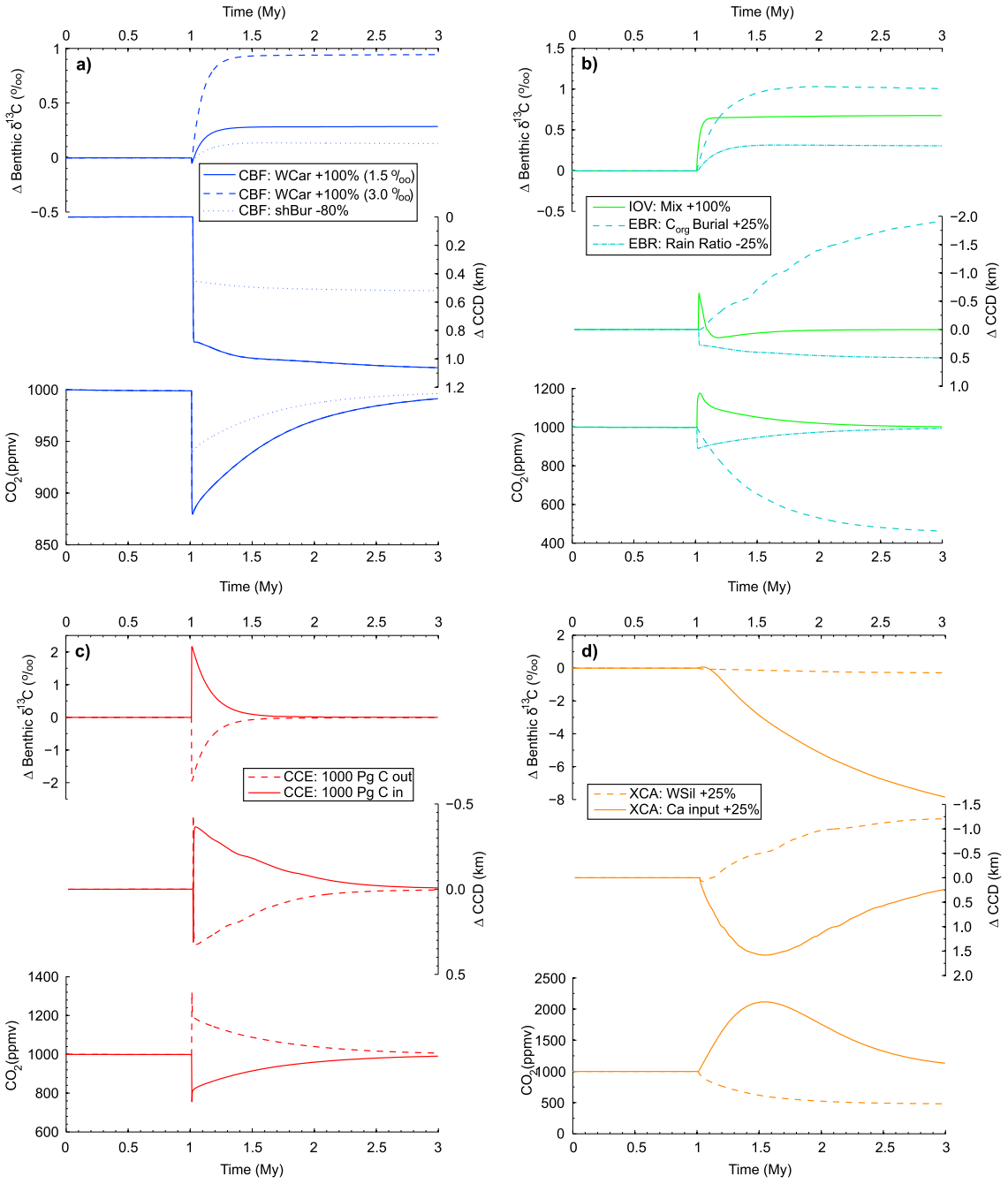

Figure 2. The results of conceptual simulations of each hypothesized mechanism in isolation to illustrate their impact on $\delta^{13}C$, the CCD, and $_{atm}CO_2$. Instantaneous step function changes in (a) carbonate weathering (WCar) and shelf carbonate burial (shBur); (b) ocean mixing rate (Mix), C_{org} burial, and rain ratio; (c) carbon capacitor exchange (Pg C in and out); and (d) silicate weathering (WSil) and calcium input (Ca input), with the hypothesis scenario in which each change is implemented within labeled. Note that the time axis is reversed relative to Figures 3–8.

representative. This 300% increase in carbonate weathering is also much greater than that estimated for the Last Glacial Maximum (20 to 27%, although shelf carbonates covered roughly 5 times more area prior to the EOT and so a proportionately greater increase is expected [*Gibbs and Kump*, 1994; *Munhoven*, 2002]) and also results in a decrease in $_{atm}CO_2$ of ~200 ppm. More seriously, this scenario demands the permanent loss of nearly all (99%) shallow-water carbonate burial, a prediction fundamentally at odds with the geological record even taking into account our very conservative baseline estimate for the shelf carbonate burial-rich Eocene [*Opdyke and Wilkinson*, 1988].

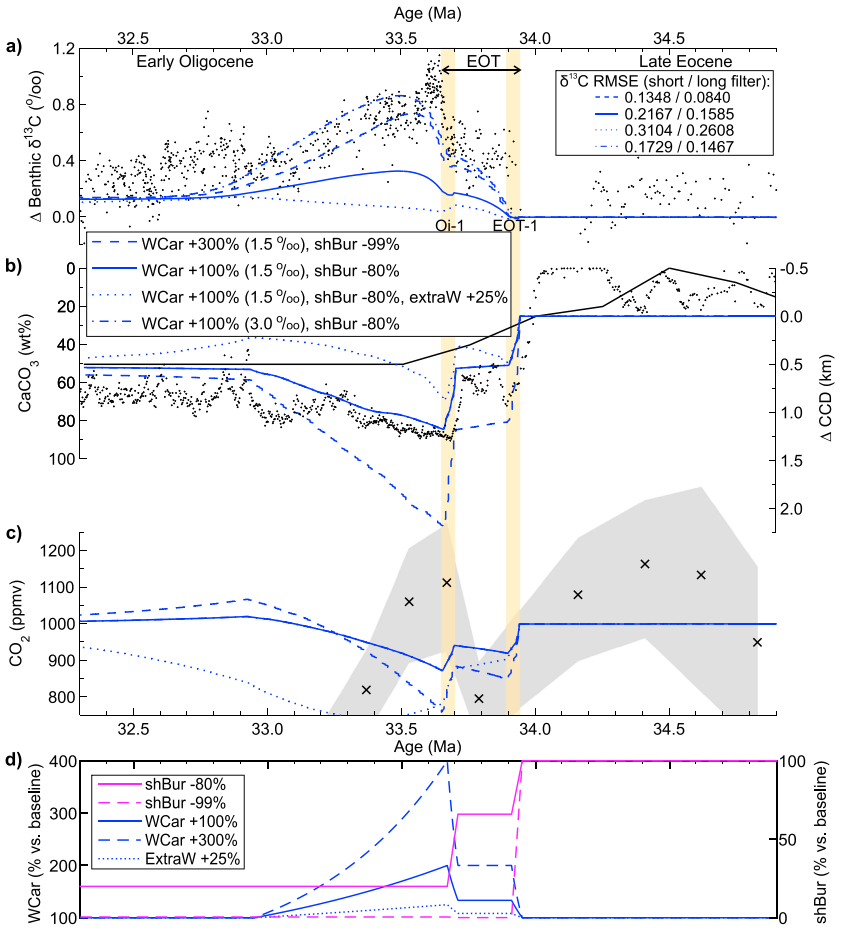

Figure 3. Simulation results for the carbonate burial fractionation (CBF) scenario. (a) Benthic $\delta^{13}C$ (with RMSE indicating model-data fit), (b) global CCD, and (c) $_{atm}CO_2$ outputs compared against EOT paleorecords (see caption of Figure 1 for details; benthic $\delta^{13}C$ and CCD have been pinned to $\Delta = 0$ at 34.0 Ma; paleorecords in black) [*Coxall et al.*, 2005; *Pearson et al.*, 2009; *Coxall and Wilson*, 2011; *Pälike et al.*, 2012; *Westerhold et al.*, 2014]. (d) The simulation scenarios are as follows: a two-step 300% increase in shelf carbonate weathering (WCar) with a $\delta^{13}C$ value of 1.5‰ coupled with a 99% reduction in shelf carbonate burial (shBur) (blue dashed line), a two-step 100% increase in shelf carbonate weathering (1.5‰) coupled with an 80% reduction in shelf carbonate burial (blue solid line), a run identical to the latter scenario but with an additional 25% increase in silicate and kerogen weathering and a 25% increase in riverine phosphate and nitrate input (extraW) (dotted blue line), and the same prior scenario again but with shelf carbonate $\delta^{13}C$ of 3.0‰ (dash-dotted blue line). The EOT-1 and Oi-1 cooling and glaciation steps within the EOT are highlighted by the yellow bars.

A more modest permanent 80% reduction (33% step at EOT-1) in shelf carbonate burial (as indicated by *Opdyke and Wilkinson* [1988]) and temporary 100% increase (33% step at EOT-1) in carbonate weathering are both more in line with the geological record and are still capable of permanently deepening the CCD by ~500 m with an initial overdeepening of a further ~500 m and a ~100 ppm decrease in $_{atm}CO_2$. On the other hand, this scenario is not capable of matching the whole $\delta^{13}C$ excursion unless the ^{13}C enrichment of shelf carbonates (see section 2.2.1) is increased from 1.5‰ to 3.0‰. This degree of enrichment is modest in comparison to that observed in the modern [*Swart and Eberli*, 2005], but more data sets are needed from shelf carbonates of Paleogene age to test the applicability of this observation to the EOT.

In these first two carbonate burial fractionation (CBF) experiments we assume that only carbonate weathering increased during the EOT. However, an associated but lower amplitude increase in noncarbonate weathering is possible [*Opdyke and Wilkinson*, 1988; *Gibbs and Kump*, 1994; *Munhoven*, 2002]. To account for the possible impact of increases in noncarbonate weathering, we also illustrate the results of a rerun of the permanent 80% shelf burial reduction and 100% increase in carbonate weathering scenario but with additional silicate and kerogen weathering and riverine nutrient input to the ocean as well. Adding a

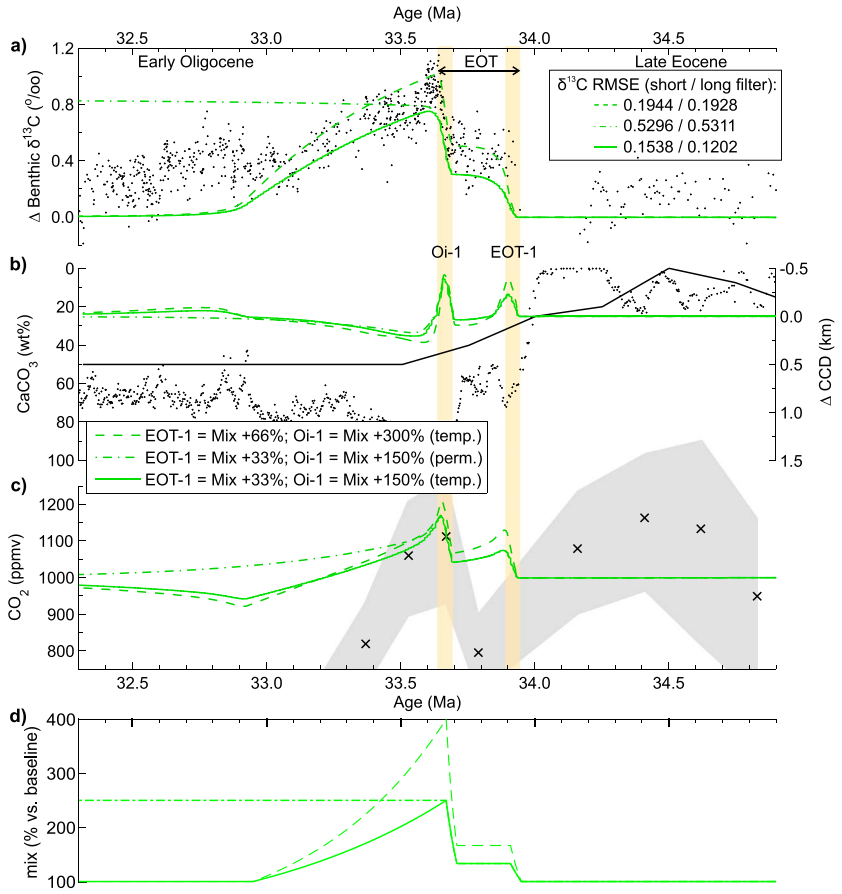

Figure 4. Simulation results for the increased ocean ventilation (IOV) scenario. (a) Benthic $\delta^{13}C$ (with RMSE indicating model-data fit), (b) global CCD, and (c) $_{atm}CO_2$ outputs compared against EOT paleorecords (see caption of Figure 2 for details) [*Coxall et al.*, 2005; *Pearson et al.*, 2009; *Coxall and Wilson*, 2011; *Pälike et al.*, 2012; *Westerhold et al.*, 2014]. (d) The simulation scenarios are as follows: a temporary two-step increase in ocean mixing rates (mix) of 66% at EOT-1 and 300% at Oi-1 (dashed green line), a permanent two-step increase in ocean mixing rates of 33% at EOT-1 and 150% at Oi-1 (dash-dotted green line), and a temporary two-step increase in ocean mixing rates of 33% at EOT-1 and 150% at Oi-1 (solid green line). The EOT-1 and Oi-1 cooling and glaciation steps within the EOT are highlighted by the yellow bars.

temporary 25% increase in silicate and kerogen weathering and a temporary 25% increase in the delivery of phosphates and nitrates by rivers (in both cases an 8.3% step at EOT-1) reduces the initial overdeepening of the CCD, almost completely attenuates the benthic $\delta^{13}C$ excursion, and results in a bigger $_{atm}CO_2$ reduction (~150 ppm larger, Figure 3). The CCD changes simulated are the result of the climate-weathering feedback resulting in additional $_{atm}CO_2$ drawdown, which in turn leads to a decrease in the global baseline weathering rate and reduced alkalinity input to the ocean. The $_{atm}CO_2$ changes are also the result of increased nutrient input resulting in a spike in primary production, which preferentially exports ^{12}C from surface to deep waters and thus helps counteract the positive $\delta^{13}C$ excursion along with the impact of higher surface $[CO_3^{2-}]$ on carbon isotope fractionation in plankton [*Spero et al.*, 1997]. Adding additional silicate and kerogen weathering therefore reduces the match to our simulation targets.

3.1.2. Increased Ocean Ventilation

Figures 2 and 4 illustrate the results of increasing ocean mixing rates, a suggested response to EOT cooling that leads to an initial reduction in vertical temperature gradients, and increased deepwater formation and overturning circulation. To match the benthic $\delta^{13}C$ paleorecord, we temporarily increase ocean mixing rates by 66% above baseline during and after EOT-1 and to 300% above baseline during Oi-1. A more modest 150% stepped increase (50% step at EOT-1) produces a smaller temporary increase in benthic $\delta^{13}C$. Neither of these simulations produces a permanently deepened CCD, because the carbonate compensation mechanism buffers deep water against permanent increases in both $[CO_3^{2-}]$ and ocean Ω through increased $CaCO_3$

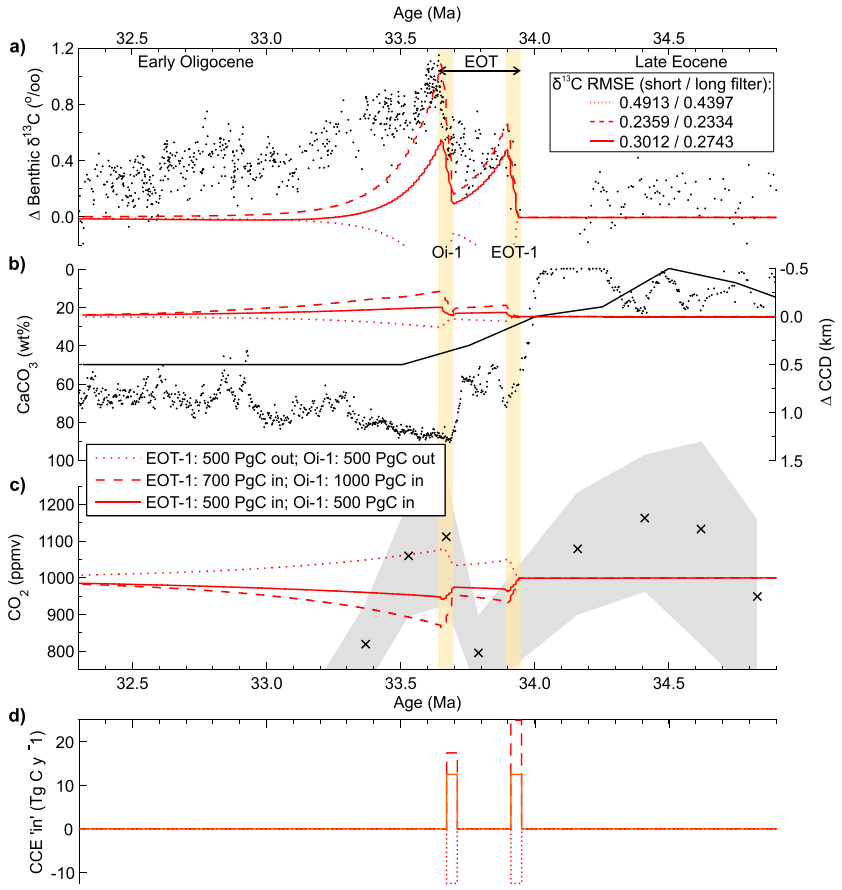

Figure 5. Simulation results for the carbon capacitor exchange (CCE) scenario. (a) Benthic $\delta^{13}C$ (with RMSE indicating model-data fit), (b) global CCD, and (c) $_{atm}CO_2$ outputs compared against EOT paleorecords (see caption of Figure 2 for details) [*Coxall et al.*, 2005; *Pearson et al.*, 2009; *Coxall and Wilson*, 2011; *Pälike et al.*, 2012; *Westerhold et al.*, 2014]. (d) The simulation scenarios are as follows: a net contraction (out) of 500 Pg C during both EOT-1 and Oi-1 (dotted red line), net expansions (in) of 700 Pg C at EOT-1 and 1000 Pg C at Oi-1 (dashed red line), and net expansions of 500 Pg C during both EOT-1 and Oi-1 (solid red line). The EOT-1 and Oi-1 cooling and glaciation steps within the EOT are highlighted by the yellow bars.

burial if $[Ca^{2+}]$ remains relatively constant, and the CCD temporarily shoals during the steps. Increasing ocean mixing rates leads to an increase in benthic foraminifera $\delta^{13}C$ as a result of the impact of permanently decreased shallow-water $[CO_3^{2-}]$ (as its concentration converges with the CO_3-poor deep ocean) on carbon isotope fractionation [*Spero et al.*, 1997]. This leads to elevated $\delta^{13}C$ in carbonate formed in the surface box and therefore an increase in ^{13}C export from the surface and an increase in the $\delta^{13}C$ of DIC in deep water. This fractionation has a greater impact than other processes that tend to lower benthic foraminifera $\delta^{13}C$. Permanently increasing mixing rates results in permanently rather than temporarily elevated benthic $\delta^{13}C$. It is clear, therefore, that suggestions of increased ocean ventilation as a mechanism for permanently deacidifying the deep ocean [e.g., *Miller et al.*, 2009] are untenable. However, increased ocean mixing is a potentially viable mechanism for driving the benthic $\delta^{13}C$ excursion. All of these simulations produce rapid ~100 ppm increases in $_{atm}CO_2$ during both cooling/glaciation steps as a result of surface water acidification, followed by a gradual recovery with a small overshoot. There is some resemblance between this recovery and the $_{atm}CO_2$ rebound seen in the $\delta^{11}B$-derived $_{atm}CO_2$ reconstruction (but not in the alkenone-derived $_{atm}CO_2$ reconstruction) for the EOT but the sparse temporal resolution and basic age control in that record do not permit further investigation.

3.1.3. Carbon Capacitor Exchange

Figures 2 and 5 illustrate the results of simulated changes in carbon capacitors across the EOT. We find that to recreate the sharp step increases in the benthic $\delta^{13}C$ paleorecord, we need to draw down 700 Pg C (at a $\delta^{13}C$

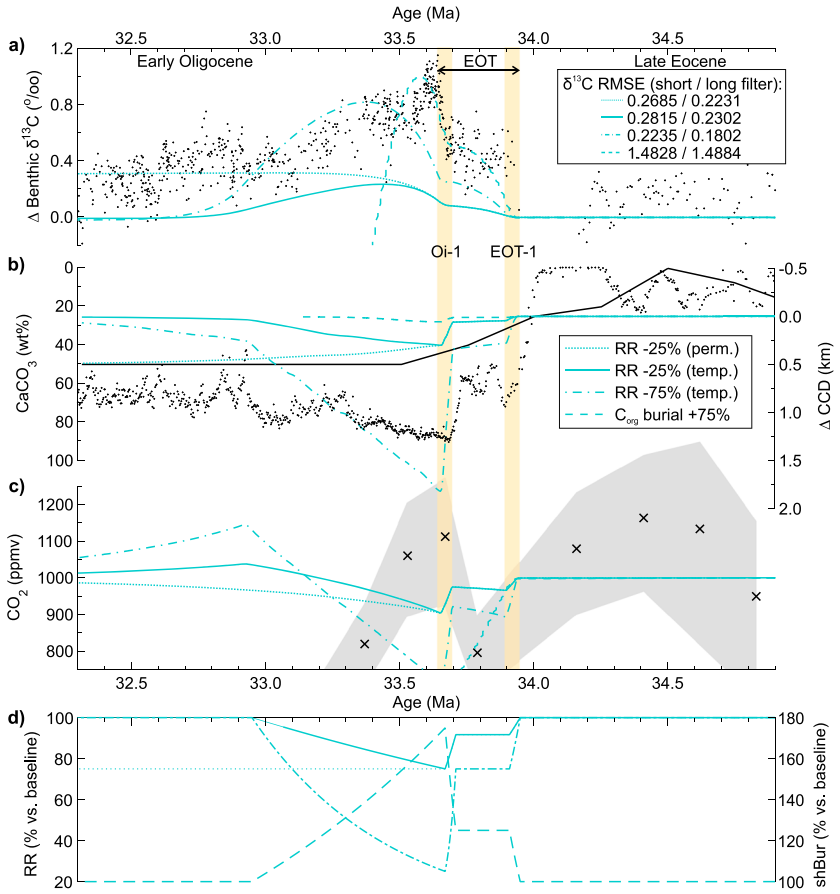

Figure 6. Simulation results for the decreased $CaCO_3$ export or increased C_{org} burial (export and burial flux changes (EBF)) scenario. (a) Benthic $\delta^{13}C$ (with RMSE indicating model-data fit), (b) global CCD, and (c) $_{atm}CO_2$ outputs compared against EOT paleorecords (see caption of Figure 2 for details) [*Coxall et al.*, 2005; *Pearson et al.*, 2009; *Coxall and Wilson*, 2011; *Pälike et al.*, 2012; *Westerhold et al.*, 2014]. (d) The simulation scenarios are as follows: a permanent two-step 25% decrease in rain ratio (RR) (dotted cyan line), a temporary two-step 25% decrease in rain ratio (solid cyan line), a temporary two-step 75% decrease in rain ratio (dash-dotted cyan line), and a permanent two-step 75% increase in C_{org} burial in sediment (dashed cyan line). The EOT-1 and Oi-1 cooling and glaciation steps within the EOT are highlighted by the yellow bars.

of −23‰) during EOT-1 and 1000 Pg C during Oi-1, but the effect of these perturbations are short lived and cannot explain the long (~1 Myr) duration of the benthic $\delta^{13}C$ excursion. A more modest uptake of 500 Pg C during both EOT-1 and Oi-1 results in rapid benthic $\delta^{13}C$ increases of ~0.5‰ during both of these events. In contrast, a net release of 500 Pg C during both EOT-1 and Oi-1, which would occur if, for example, more carbon is released by PFSC erosion on Antarctica than is taken up into carbon capacitor expansion elsewhere, results in decreases in benthic $\delta^{13}C$ in contrast to the sharp positive excursions seen in the paleorecord. Because of the relatively small mass of carbon required to simulate the carbon isotope perturbation, capacitor exchange leading to a match with the $\delta^{13}C$ data has a relatively minor impact on the CCD and $_{atm}CO_2$ (the former shoaling by ~100 m and the latter decreasing by ~50 ppm by the end of Oi-1 in the modest uptake scenario).

3.1.4. Export and Burial Flux Changes

Figures 2 and 6 illustrate the results of either reducing $CaCO_3$ export and burial by reducing the rain ratio or increasing the proportion of C_{org} preserved in ocean sediment in order to increase C_{org} burial. A permanent 25% decrease in rain ratio (8.3% step at EOT-1) results in a permanent 500 m deepening of the CCD and a permanent ~0.3‰ increase in benthic $\delta^{13}C$ (contrasting with the largely temporary $\delta^{13}C$ excursion of the paleorecord) along with $_{atm}CO_2$ temporarily falling by ~100 ppm. A temporary benthic $\delta^{13}C$ excursion can be achieved with a temporary rain ratio decrease, but this fails to produce a permanently deepened CCD. To achieve a ~0.7‰ increase in benthic $\delta^{13}C$, the rain ratio must decrease by ~75% (25% step at EOT-1),

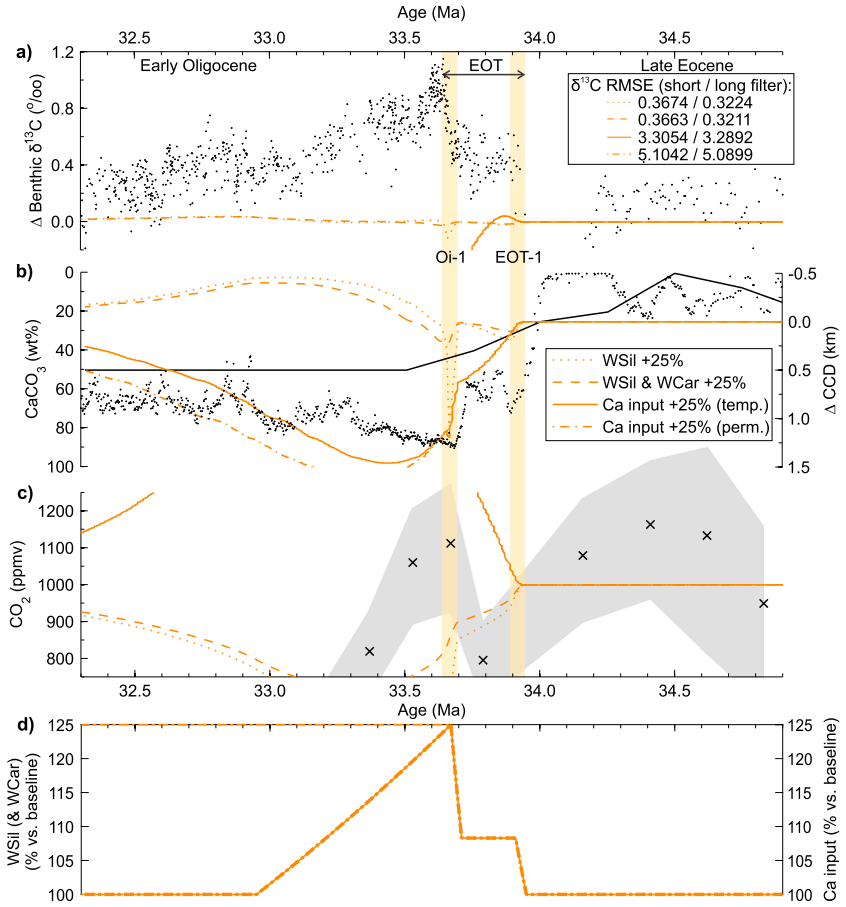

Figure 7. Simulation results for the silicate weathering and calcium (SWC) scenario. (a) Benthic $\delta^{13}C$ (with RMSE indicating model-data fit), (b) global CCD, and (c) $_{atm}CO_2$ outputs compared against EOT paleorecords (see caption of Figure 2 for details) [*Coxall et al.*, 2005; *Pearson et al.*, 2009; *Coxall and Wilson*, 2011; *Pälike et al.*, 2012; *Westerhold et al.*, 2014]. (d) The simulation scenarios are as follows: a permanent two-step 25% increase in calcium input (Ca input) (dash-dotted orange line), a temporary two-step 25% increase in calcium input (solid orange line), a temporary two-step 25% increase in silicate weathering rates (WSil) (dotted orange line), and a temporary two-step 25% increase in both silicate and carbonate weathering (WCar) rates (dashed orange line). The EOT-1 and Oi-1 cooling and glaciation steps within the EOT are highlighted by the yellow bars.

which also results in a >1.5 km temporary deepening of the CCD and a temporary ~300 ppm drop in $_{atm}CO_2$. This result shows that a significant positive benthic $\delta^{13}C$ excursion can only be achieved through a substantial decrease in the rain ratio, which conflicts with paleorecords [*Griffith et al.*, 2010].

In a second experiment we increase the proportion of C_{org} buried in sediments by 75% (25% step at EOT-1) to try to replicate the >0.7‰ benthic $\delta^{13}C$ excursion, but this in turn results in a significant decrease in both DIC and alkalinity concentration as total carbon output exceeds input and the complete consumption of $_{atm}CO_2$ by ~33.1 Ma. Simulated benthic foraminiferal $\delta^{13}C$ initially increases as a result of ^{12}C removal from the ocean via increased C_{org} burial, but this is followed by a large negative excursion as a result of the effect on $\delta^{13}C$ fractionation of intense ocean deacidification. The CCD shows a negligible and temporary deepening because of increasing $[CO_3^{2-}]$ that is attributable to DIC drawdown-induced deacidification. This effect initially outpaces the influence of decreasing $[Ca^{2+}]$ (due to weathering inputs decreasing with falling $_{atm}CO_2$) and K_{sp} to temporarily increase deepwater saturation state, but this is followed by more significant impacts on the ocean carbonate system as intense DIC drawdown progresses.

3.1.5. Increased Silicate Weathering and Calcium Flux to the Ocean

Figures 2 and 7 illustrate the results of adding additional silicate weathering or directly adding Ca^{2+} to the ocean in order to match the EOT paleorecords. In the first of these experiments a 25% increase in silicate

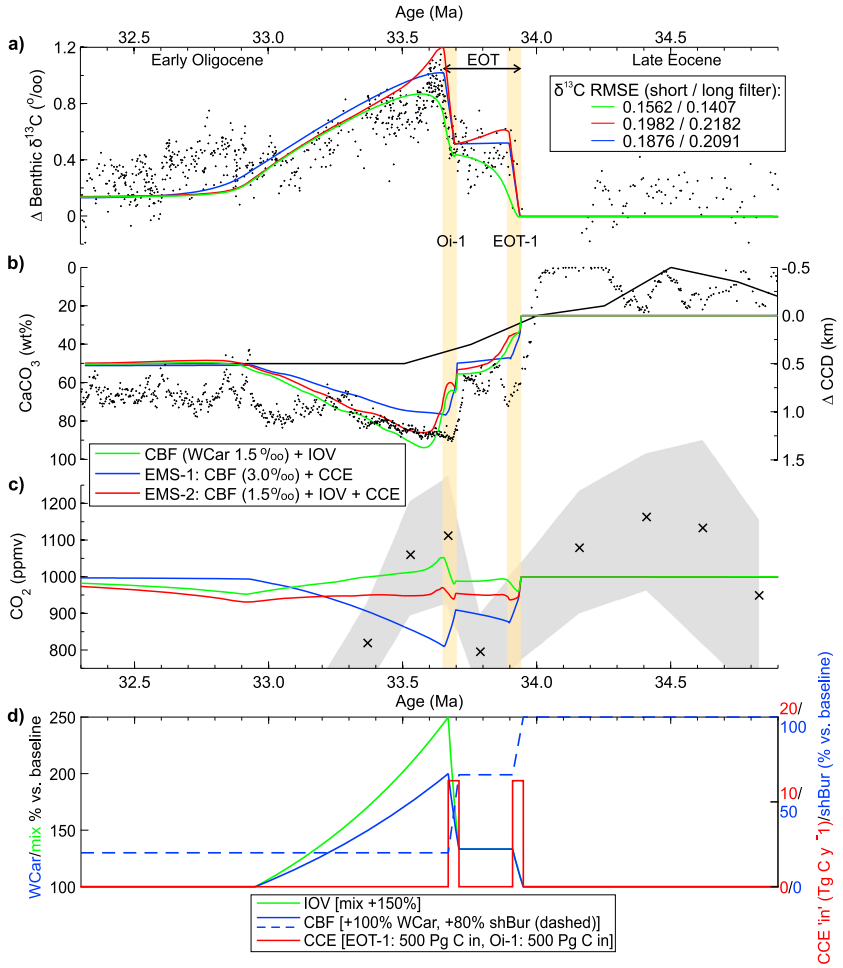

Figure 8. Simulation results of (a) benthic $\delta^{13}C$ (with RMSE indicating model-data fit), (b) global CCD, and (c) $_{atm}CO_2$ for the different combinations of the best fit scenarios shown in previous figures compared against EOT paleorecords (see caption of Figure 2 for details) [*Coxall et al.*, 2005; *Pearson et al.*, 2009; *Coxall and Wilson*, 2011; *Pälike et al.*, 2012; *Westerhold et al.*, 2014]; (d) Best fit simulation scenarios: CBF (WCar 1.5‰) + IOV, green; end-member scenario 1: CBF (WCar 1.5‰) + IOV + CCE, red; end-member scenario 2: CBF (WCar 3.0‰) + CCE, blue. The EOT-1 and Oi-1 cooling and glaciation steps within the EOT are highlighted by the yellow bars.

weathering (added separately from the baseline global weathering rate to represent the source as increased weatherability; 8.3% step at EOT-1) is added across the EOT in order to both draw down $_{atm}CO_2$ and increase the input of Ca^{2+} and bicarbonate to the ocean and deepen the CCD. However, in our simulations the decrease in $_{atm}CO_2$ is sufficient to suppress the global baseline weathering rate, thereby compensating for elevated shelf weatherability by reducing silicate weathering rates elsewhere. This also acts to relax the global carbonate weathering rate, which in turn results in a net decrease in alkalinity input and therefore CCD shoaling instead of deepening. Adding additional carbonate weathering by the same proportion as the additional silicate weathering fails to compensate for the impact of lowered $_{atm}CO_2$ and results in similar excursions. Removing the climate-weathering feedback by preventing the decline in global baseline weathering rates in response to declining $_{atm}CO_2$ instead results in a temporary CCD deepening (see supporting information Figure S2). As a result it is clear that in keeping with the results of *Merico et al.* [2008] any additional input of Ca^{2+} and alkalinity to the ocean attributable to an increase in silicate weathering is strongly counteracted by the climate-weathering negative feedback.

In a further experiment we isolate the impact of increasing $[Ca^{2+}]$ by adding Ca^{2+} to the ocean without increasing either silicate or carbonate weathering. We find that in order to initially deepen the CCD by

~1000 m, [Ca^{2+}] must increase by a factor of 8 from ~20 to ~170 mol m^{-3} (a value at odds with reconstructions of past [Ca^{2+}]), which requires Ca^{2+} input to the ocean to temporarily increase by 25% (8.3% step at EOT-1). Furthermore, CCD deepening is only temporary and is accompanied by a ~4.0‰ decrease in benthic $\delta^{13}C$ and a >700 ppm increase in $_{atm}CO_2$, signals that are untenable in light of the paleorecord. Applying a permanent increase in Ca^{2+} input to the ocean also fails to result in a permanent CCD deepening and results in even more unrealistic changes in ocean [Ca^{2+}], benthic $\delta^{13}C$, and $_{atm}CO_2$. The extreme benthic $\delta^{13}C$ and atmospheric CO_2 excursions are driven by a complex set of feedbacks on the initial Ca^{2+} addition (see supporting information Text S2 and Figure S3 for explanation of these feedbacks).

3.1.6. Combined Scenarios

In Figure 8 we plot simulations that combine the mechanisms that we judge to best fit the paleorecords within reasonable parameter changes. The combined CBF-IOV (increased ocean ventilation) experiment (80% reduction in shelf carbonate burial, temporary 100% stepped increase in carbonate weathering, shelf carbonate $\delta^{13}C$ of 1.5‰, and temporary 150% stepped increase in ocean mixing rates) results in both a permanent ~500 m deepening of the CCD, with an initial overdeepening of ~1000 m, and a temporary ~0.6‰ benthic $\delta^{13}C$ excursion featuring two steps, as seen in the paleorecords. Adding CCE (500 Pg C drawdown during both EOT-1 and Oi-1) to this experiment accentuates the two steps in the benthic $\delta^{13}C$ excursion making them more rapid and briefly increases the benthic $\delta^{13}C$ excursion to ~1.0‰ during Oi-1, fitting the maximum shift observed in the benthic $\delta^{13}C$ paleorecord. This experiment also produces a small ~50 ppm decline in $_{atm}CO_2$ after EOT-1. Alternatively, by increasing shelf carbonate ^{13}C enrichment to 3.0‰, we are able to match both the benthic $\delta^{13}C$ and CCD paleorecords using a combination of CBF and CCE without also including IOV. This enriched CBF and CCE scenario is the only experiment of these combination runs that results in a major (~190 ppm) decline in $_{atm}CO_2$. All of the above simulations produce good model-data fits for benthic $\delta^{13}C$ as quantified by RMSE, and although a slightly worse RMSE results from adding CCE, we note that the data filtering undertaken prior to quantifying the RMSE smoothes out the steps and thus the RMSE is unlikely to accurately quantify model-data fit during these very rapid steps.

3.2. Implications

3.2.1. Combined Drivers Lead to Best Model-Data Fit

We find that no one hypothesis can completely achieve our two simulation targets of a permanent 500 m long-term deepening of the CCD with an initial overdeepening of ≤1200 m and a temporary > +0.7‰ benthic $\delta^{13}C$ excursion with rapid 40 kyr steps at EOT-1 and Oi-1. Of our experiments, only a permanent 80% reduction in shallow ocean carbonate burial (Figure 3) or a permanent 25% decrease in rain ratio (Figure 6) matches the long-term CCD deepening (but the latter does not match the initial overdeepening). On the other hand, only a 150 to 300% increase in ocean mixing rates (Figure 4), a 300% increase in shelf carbonate weathering with a $\delta^{13}C$ of 1.5‰ (Figure 3), a 100% increase in shelf carbonate weathering with a $\delta^{13}C$ of 3.0‰ (Figure 3), or a temporary 75% decrease in rain ratio (Figure 6) matches the magnitude, but not quite the rapidity, of the benthic $\delta^{13}C$ target. A 75% increase in C_{org} burial (Figure 6) can also match the benthic $\delta^{13}C$ excursion in magnitude and rapidity but ultimately results in model failure due to complete $_{atm}CO_2$ drawdown. Carbon capacitor expansion of ~1000 Pg C (Figure 5) reproduces the rapidity of the 40 kyr steps but not the overall duration and magnitude of the benthic $\delta^{13}C$ excursion. Because a decrease in the rain ratio cannot achieve both simulation targets simultaneously and Ca isotope evidence suggests that the rain ratio is more likely to have increased rather than decreased across the EOT [*Griffith et al.*, 2010], we conclude that changes in the rain ratio did not play a major role in driving the EOT carbon cycle perturbation, although it could play a minor role in amplifying the excursion and maintaining slightly higher than pre-EOT benthic $\delta^{13}C$ after the EOT.

It is highly implausible that increases in silicate weathering or ocean [Ca^{2+}] drove the EOT perturbation because of the extreme mismatches between simulation results and the paleorecords and the infeasible scale and rate of the changes required (severalfold changes within a few 100 kyr when the residence time is ~1 Myr) (Figure 7). A 300% increase in carbonate weathering overdeepens the CCD by far more than observed in the paleorecords, indicating that only a more modest increase in carbonate weathering can be accommodated [*Rea and Lyle*, 2005; *Pälike et al.*, 2012]. The limited data available for shelf carbonate $\delta^{13}C$ indicates Eocene-Oligocene values of around 1.5 to 2.5‰ compared with deep sea sediment values of ~0.5‰ [*Zachos et al.*, 2001; *Swart and Eberli*, 2005], but modern shelf carbonates, for example, on the relatively globally representative Great Bahama Bank, are enriched by ~4.8‰ relative to pelagic carbonate

[*Swart*, 2008; *Swart et al*., 2009; *Oehlert et al*., 2012]. We therefore define two possible end-member scenarios that can achieve both of our simulation targets. End-member scenario 1 describes a situation in which shelf carbonate is relatively ^{13}C-enriched (~3.0‰) meaning that a combination of carbonate burial fractionation (CBF; Figure 3) and carbon capacitor expansion (CCE; Figure 5) is sufficient to match the paleoclimate record. End-member scenario 2 describes a situation in which shelf carbonate is less ^{13}C-enriched (~1.5‰) and a combination of carbonate burial fractionation (CBF; Figure 3), increased ocean ventilation (IOV; Figure 4), and carbon capacitor expansion (CCE; Figure 5) is required. New data sets of δ^{13}C in shelf carbonates of Paleogene age would provide a way to test the validity of these two end-members and the quite different predictions that they make for the drivers of change in $_{atm}CO_2$ across the EOT (see 3.2.3).

3.2.2. Carbon Capacitor Expansion Across the EOT

Sequestering carbon at a modest rate from the atmosphere into C_{org} reservoirs during EOT-1 and Oi-1 helps to create rapid steps in the benthic δ^{13}C excursion in our best fit simulation (Figure 8). No other mechanism tested was able to reproduce the rapidity of these steps. Our results therefore suggest that isotopically light carbon might have been rapidly sequestered from the ocean-atmosphere system to carbon capacitors during the EOT. One mechanism to explain such large-scale sequestration over such a short timescale is through expansion of the permafrost and global peatlands inventories in the Northern Hemisphere in response to EOT cooling, which modeling suggests can occur within 1 to 10 kyr [*Klinger et al*., 1996; *Tarnocai et al*., 2009; *DeConto et al*., 2012]. Up to ~1700 Pg C is thought to have existed in Antarctic permafrost in the Eocene [*DeConto et al*., 2012]. The absence of an overall negative δ^{13}C excursion during the EOT implies that Antarctic PFSC was sequestered below advancing ice sheets, rapidly redeposited offshore, or partially eroded prior to the EOT, consistent with some evidence [*Coxall and Wilson*, 2011] for a negative δ^{13}C excursion before EOT-1. Further constraints on the behavior of the PFSC and peatland reservoirs during the EOT are required to further test this hypothesis.

3.2.3. Atmospheric CO_2 and Glaciation Feedbacks

End-member scenario 2 involving only modest shelf carbonate ^{13}C-enrichment (Figure 8) results in only small changes in $_{atm}CO_2$ across the EOT. This finding is important because, if shelf carbonate enrichment was small, it suggests against the operation of a strong $_{atm}CO_2$ positive feedback on EOT glaciation. Maintenance of high baseline $_{atm}CO_2$ levels across the EOT may help to explain the ice sheet instability implied by high amplitude variability in the early Oligocene benthic oxygen isotope record [*Coxall et al*., 2005]. These findings conflict with low-resolution $_{atm}CO_2$ reconstructions based on boron isotope [*Pearson et al*., 2009] and carbon isotope fractionation [*Heureux and Rickaby*, 2015] data which suggest that $_{atm}CO_2$ initially decreased across EOT-1 (by ~200 ppm in the boron reconstruction) before rapidly increasing during Oi-1 (by 300–400 ppm in the boron reconstruction), with levels remaining high for ~200 to 500 kyr before falling below pre-EOT levels. Having simulated changes in many of the major biogeochemical parameters hypothesized to have been affected during the EOT, we find that the pattern of $_{atm}CO_2$ changes shown in the boron paleorecord is challenging to explain alongside the benthic δ^{13}C and CCD paleorecords via the hypotheses so far proposed for the EOT carbon cycle perturbation. One potential explanation for this finding is that a regional process, for example, sea ice expansion in the Southern Ocean in response to the development of a large East Antarctic Ice Sheet [*DeConto et al*., 2007; *Goldner et al*., 2014], or another process not included in our model, for example, in the terrestrial biosphere or heterogeneous climate and weathering changes, plays an important role in determining the evolution of CO_2 across the EOT. Even so, a 200 to 500 kyr long $_{atm}CO_2$ peak after Oi-1 would be challenging to maintain through ocean processes given an ocean mixing timescale of ~1 kyr. An alternative $_{atm}CO_2$ reconstruction based on alkenones suggests that $_{atm}CO_2$ permanently fell by ~200 ppm across the EOT with a potential temporary overshoot at ~33.0 Ma which is interpreted to indicate a major increase in silicate weathering across the EOT [*Pagani et al*., 2011]. We find, however, that a major increase in silicate weathering is incompatible with the sign of the CCD response and the amplitude of the carbon isotope excursion (see section 3.1.1). In contrast, end-member scenario 1 results in a major (~190 ppm) but temporary decrease in $_{atm}CO_2$ during the EOT (Figure 8). This is in line with the first ~500 kyr of the alkenone $_{atm}CO_2$ reconstruction and would also result in a positive feedback on glaciation in the early Oligocene. This suggests that under end-member scenario 1 carbonate burial fractionation may have helped drive the initial $_{atm}CO_2$ decline observed during the EOT in the alkenone reconstruction but that different processes made this decline permanent after ~500 kyr. Our study underscores the need for new multiproxy high-resolution reconstructions of $_{atm}CO_2$ across the EOT.

3.2.4. Why Was the EOT a Unique Event?

The carbon cycle perturbation at the EOT is unique in the Cenozoic. No other event involves a permanent shift in ocean carbonate burial of a similar magnitude [*Opdyke and Wilkinson*, 1988]. However, the mechanisms proposed to explain the EOT carbon cycle perturbation are likely to have been at work throughout much of the Cenozoic. Some paleorecords suggest that there were many rapid changes in sea level across the Cenozoic that did not result in a major shift in the locus of ocean carbonate burial [*Miller et al*., 2009]. In comparison to the variability demonstrated during the Eocene, the CCD remains relatively stable in the equatorial Pacific after the EOT despite fluctuations in Oligocene ice sheets and temperatures [*Palike et al*., 2006; *Pälike et al*., 2012]. CCD stability was only interrupted in the mid-Miocene, by the shoaling and subsequent redeepening of the CCD potentially associated with the deglaciation and reglaciation bracketing the Miocene Climatic Optimum [*Lyle*, 2003; *Armstrong McKay et al*., 2014]. This observation implies that post-EOT fluctuations in sea level and climate mostly failed to restore Eocene levels of shelf carbonate burial, suggesting that a threshold in the ocean carbonate system may have been crossed at the EOT beyond which a substantial fraction of carbonate burial permanently shifted to ocean basin settings. We conclude that the late Eocene ocean carbonate system was more sensitive to changing carbonate burial rates because of (1) the relative abundance of carbonate platforms in shallow tropical epicontinental seas in the Eocene within 50–75 m of sea level [*Opdyke and Wilkinson*, 1988] and (2) the relatively shallow position of the CCD poised some way above the abyssal plain where the greatest surface area is available for carbonate burial and where the CCD is therefore more buffered against change [*Pälike et al*., 2012]. Future research is needed to quantify the changing sensitivity of the CCD to sea level and climate change during the Cenozoic.

4. Conclusions

We revisit the EOT carbon cycle perturbation modeling of *Merico et al*. [2008] in light of critiques of the main carbonate burial fractionation hypothesis and our development of some new hypotheses. We use the same biogeochemical box model developed by *Merico et al*. [2008] with some additions in order to further investigate the hypothesized drivers of the perturbation. We find that in keeping with *Merico et al*. [2008], a shift in carbonate burial from shallow to deep water settings is the most likely process for permanently deepening the CCD. On the other hand, in contrast to *Merico et al*. [2008], we conclude that the form of the overall EOT benthic $\delta^{13}C$ excursion can only have been brought about by a shelf-to-basin carbonate shift if contemporaneous shelf carbonates were substantially enriched in ^{13}C (with a $\delta^{13}C$ of ~3.0‰). If this was not the case, then a contribution from increased ocean ventilation is also required. Substantial increases in silicate weathering, direct addition of Ca^{2+} to the ocean, decreasing the $CaCO_3$ flux, and increasing C_{org} burial all contradict or, at best, fail to reproduce the observations and are therefore unlikely to have played a major role at the EOT. We find that the rapidity of the two steps in the benthic $\delta^{13}C$ paleorecord can best be attributed to the net sequestration of ~1000 Pg of organic carbon during the EOT through processes such as permafrost and peatland expansion. Antarctic permafrost soil carbon must have either been sequestered by advancing ice sheets or eroded and oxidized prior to the EOT. We struggle to simulate the excursions in the boron isotope-based EOT $_{atm}CO_2$ reconstruction [*Pearson et al*., 2009]. In our model runs that fit existing data sets most closely, $_{atm}CO_2$ either remains relatively stable or shows a major (but temporary) decrease across the EOT, a result that better matches the alkenone-based EOT $_{atm}CO_2$ reconstruction [*Pagani et al*., 2011].

Acknowledgments

This work was supported by a Natural Environment Research Council (NERC) studentship to D.I.A.M. (NE/J500112/1). We thank Agostino Merico for sharing the model developed in *Merico et al*. [2008]. The paleorecords used in this study can be found at the following locations: benthic isotopes and $CaCO_3$ wt % from ODP site 1218 are available from Helen Coxall (helen.coxall@geo.su.se), the CCD in the equatorial Pacific is available from http://www.nature.com/nature/journal/v488/n7413/extref/nature11360-s1.pdf, and the boron isotope-based atmospheric CO_2 reconstruction is available from http://doi.pangaea.de/10.1594/PANGAEA.815855. This work was inspired by paleorecords produced using material obtained by the (Integrated) Ocean Drilling Program (International Ocean Discovery Program), which is sponsored by the U.S. National Science Foundation and participating countries (UK through a NERC Research Program) under management of Joint Oceanographic Institutions, Inc.

References

Armstrong McKay, D. I., T. Tyrrell, P. A. Wilson, and G. L. Foster (2014), Estimating the impact of the cryptic degassing of large igneous provinces: A mid-Miocene case-study, *Earth Planet. Sci. Lett.*, *403*, 254–262, doi:10.1016/j.epsl.2014.06.040.

Basak, C., and E. E. Martin (2013), Antarctic weathering and carbonate compensation at the Eocene–Oligocene transition, *Nat. Geosci.*, *6*(2), 121–124, doi:10.1038/ngeo1707.

Batjes, N. H. (1996), Total carbon and nitrogen in the soils of the world, *Eur. J. Soil Sci.*, *47*(2), 151–163, doi:10.1111/j.1365-2389.1996.tb01386.x.

Ben-Yaakov, S., and M. B. Goldhaber (1973), The influence of seawater composition on the apparent constants of the carbonate system, *Deep Sea Res.*, *20*, 87–99.

Berger, W. H. (2007), Cenozoic cooling, Antarctic nutrient pump, and the evolution of whales, *Deep Sea Res. Part II*, *54*(21–22), 2399–2421, doi:10.1016/j.dsr2.2007.07.024.

Berger, W. H., and E. L. Winterer (1975), Plate stratigraphy and the fluctuating carbonate line, in *Pelagic Sediments on Land and Under the Sea*, edited by K. J. Hsü and H. C. Jenkyns, pp. 11–48, Blackwell Publishers Ltd., Oxford, U. K.

Bierman, P. R., L. B. Corbett, J. A. Graly, T. A. Neumann, A. Lini, B. T. Crosby, and D. H. Rood (2014), Preservation of a preglacial landscape under the center of the Greenland Ice Sheet, *Science*, *344*(6182), 402–5, doi:10.1126/science.1249047.

Bohaty, S. M., J. C. Zachos, and M. L. Delaney (2012), Foraminiferal Mg/Ca evidence for Southern Ocean cooling across the Eocene–Oligocene transition, *Earth Planet. Sci. Lett.*, *317–318*, 251–261, doi:10.1016/j.epsl.2011.11.037.
Broecker, W. S., and T.-H. Peng (1982), *Tracers in the Sea*, Lamont-Doherty Geological Observatory, Palisades, N. Y.
Buffett, B., and D. Archer (2004), Global inventory of methane clathrate: Sensitivity to changes in the deep ocean, *Earth Planet. Sci. Lett.*, *227*(3–4), 185–199, doi:10.1016/j.epsl.2004.09.005.
Chuck, A., T. Tyrrell, I. J. Totterdell, and P. M. Holligan (2005), The oceanic response to carbon emissions over the next century: Investigation using three ocean carbon cycle models, *Tellus B*, *57*(1), 70–86, doi:10.1111/j.1600-0889.2005.00127.x.
Coxall, H. K., and P. A. Wilson (2011), Early Oligocene glaciation and productivity in the eastern equatorial Pacific: Insights into global carbon cycling, *Paleoceanography*, *26*, PA2221, doi:10.1029/2010PA002021.
Coxall, H. K., P. A. Wilson, H. Pälike, C. H. Lear, and J. Backman (2005), Rapid stepwise onset of Antarctic glaciation and deeper calcite compensation in the Pacific Ocean, *Nature*, *433*(7021), 53–57, doi:10.1038/nature03135.
De Boer, B., R. S. W. Van de Wal, R. Bintanja, L. J. Lourens, and E. Tuenter (2010), Cenozoic global ice-volume and temperature simulations with 1-D ice-sheet models forced by benthic $\delta^{18}O$ records, *Ann. Glaciol.*, *51*(55), 23–33, doi:10.3189/172756410791392736.
De La Rocha, C. L. (2000), Isotopic evidence for variations in the marine calcium cycle over the Cenozoic, *Science*, *289*(5482), 1176–1178, doi:10.1126/science.289.5482.1176.
DeConto, R. M., and D. Pollard (2003), Rapid Cenozoic glaciation of Antarctica induced by declining atmospheric CO_2, *Nature*, *421*(6920), 245–9, doi:10.1038/nature01290.
DeConto, R. M., D. Pollard, and D. M. Harwood (2007), Sea ice feedback and Cenozoic evolution of Antarctic climate and ice sheets, *Paleoceanography*, *22*, PA3214, doi:10.1029/2006PA001350.
DeConto, R. M., S. Galeotti, M. Pagani, D. Tracy, K. Schaefer, T. Zhang, D. Pollard, and D. J. Beerling (2012), Past extreme warming events linked to massive carbon release from thawing permafrost, *Nature*, *484*(7392), 87–91, doi:10.1038/nature10929.
Dickens, G. R. (2011), Down the rabbit hole: Toward appropriate discussion of methane release from gas hydrate systems during the Paleocene-Eocene thermal maximum and other past hyperthermal events, *Clim. Past*, *7*(3), 831–846, doi:10.5194/cp-7-831-2011.
Dunkley Jones, T., P. R. Bown, P. N. Pearson, B. S. Wade, H. K. Coxall, and C. H. Lear (2008), Major shifts in calcareous phytoplankton assemblages through the Eocene-Oligocene transition of Tanzania and their implications for low-latitude primary production, *Paleoceanography*, *23*, PA4204, doi:10.1029/2008PA001640.
Fantle, M. S. (2010), Evaluating the Ca isotope proxy, *Am. J. Sci.*, *310*(3), 194–230, doi:10.2475/03.2010.03.
Farkaš, J., F. Böhm, K. Wallmann, J. Blenkinsop, A. Eisenhauer, R. van Geldern, A. Munnecke, S. Voigt, and J. Veizer (2007a), Calcium isotope record of Phanerozoic oceans: Implications for chemical evolution of seawater and its causative mechanisms, *Geochim. Cosmochim. Acta*, *71*(21), 5117–5134, doi:10.1016/j.gca.2007.09.004.
Farkaš, J., D. Buhl, J. Blenkinsop, and J. Veizer (2007b), Evolution of the oceanic calcium cycle during the late Mesozoic: Evidence from $\delta^{44/40}Ca$ of marine skeletal carbonates, *Earth Planet. Sci. Lett.*, *253*(1–2), 96–111, doi:10.1016/j.epsl.2006.10.015.
Gibbs, M. T., and L. R. Kump (1994), Global chemical erosion during the last glacial maximum and the present: Sensitivity to changes in lithology and hydrology, *Paleoceanography*, *9*(4), 529–543.
Goldner, A., N. Herold, and M. Huber (2014), Antarctic glaciation caused ocean circulation changes at the Eocene–Oligocene transition, *Nature*, *511*(7511), 574–577, doi:10.1038/nature13597.
Griffith, E. M., M. Calhoun, E. Thomas, K. Averyt, T. J. Bralower, M. W. Lyle, A. Olivarez-lyle, and A. Paytan (2010), Export productivity and carbonate accumulation in the Pacific basin at the transition from a greenhouse to icehouse climate (late Eocene to early Oligocene), *Paleoceanography*, *25*, PA3212, doi:10.1029/2010PA001932.
Griffith, E. M., A. Paytan, A. Eisenhauer, T. D. Bullen, and E. Thomas (2011), Seawater calcium isotope ratios across the Eocene-Oligocene transition, *Geology*, *39*(7), 683–686, doi:10.1130/G31872.1.
Hain, M. P., D. M. Sigman, J. A. Higgins, and G. H. Haug (2015), The effects of secular calcium and magnesium concentration changes on the thermodynamics of seawater acid/base chemistry: Implications for Eocene and Cretaceous ocean carbon chemistry and buffering, *Global Biogeochem. Cycles*, *29*, 517–533, doi:10.1002/2014GB004986.
Heureux, A. M. C., and R. E. M. Rickaby (2015), Refining our estimate of atmospheric CO_2 across the Eocene–Oligocene climatic transition, *Earth Planet. Sci. Lett.*, *409*, 329–338, doi:10.1016/j.epsl.2014.10.036.
Heuser, A., A. Eisenhauer, F. Böhm, K. Wallmann, N. Gussone, P. N. Pearson, T. F. Nägler, and W. C. Dullo (2005), Calcium isotope ($\delta^{44/40}Ca$) variations of Neogene planktonic foraminifera, *Paleoceanography*, *20*, PA2013, doi:10.1029/2004PA001048.
Houben, A. J. P., C. A. van Mourik, A. Montanari, R. Coccioni, and H. Brinkhuis (2012), The Eocene-Oligocene transition: Changes in sea level, temperature or both?, *Palaeogeogr. Palaeoclimatol. Palaeoecol.*, *335–336*, 75–83, doi:10.1016/j.palaeo.2011.04.008.
John, E. H., J. D. Wilson, P. N. Pearson, and A. Ridgwell (2014), Temperature-dependent remineralization and carbon cycling in the warm Eocene oceans, *Palaeogeogr. Palaeoclimatol. Palaeoecol.*, *413*, 158–166, doi:10.1016/j.palaeo.2014.05.019.
Kennett, J., and N. Shackleton (1976), Oxygen isotopic evidence for the initiation of the psychrosphere 38 Myr ago, *Nature*, *260*, 513–515.
Kennett, J. P. (1977), Cenozoic evolution of Antarctic glaciation, the circum-Antarctic Ocean, and their impact on global paleoceanography, *J. Geophys. Res.*, *82*(27), 3843–3860.
Klinger, L. F. (1991), Peatland formation and ice ages: A possible Gaian mechanism related to community succession, in *Scientists on Gaia*, edited by S. Schneider and P. Boston, pp. 247–255, MIT Press, Cambridge, Mass.
Klinger, L. F., J. A. Taylor, and L. G. Franzen (1996), The potential role of peatland dynamics in ice-age initiation, *Quat. Res.*, *45*(1), 89–92, doi:10.1006/qres.1996.0008.
Komar, N., and R. E. Zeebe (2011), Oceanic calcium changes from enhanced weathering during the Paleocene-Eocene thermal maximum: No effect on calcium-based proxies, *Paleoceanography*, *26*, PA3211, doi:10.1029/2010PA001979.
Koven, C. D., B. Ringeval, P. Friedlingstein, P. Ciais, P. Cadule, D. Khvorostyanov, G. Krinner, and C. Tarnocai (2011), Permafrost carbon-climate feedbacks accelerate global warming, *Proc. Natl. Acad. Sci. U.S.A.*, *108*, 14,769–14,774, doi:10.1073/pnas.1103910108.
Kump, L. R., and M. A. Arthur (1997), Global chemical erosion during the Cenozoic: Weatherability balances the budgets, in *Tectonic Uplift and Climate Change*, edited by W. F. Ruddiman, pp. 399–426, Springer US, Boston, Mass.
Ladant, J.-B., Y. Donnadieu, V. Lefebvre, and C. Dumas (2014), The respective role of atmospheric carbon dioxide and orbital parameters on ice sheet evolution at the Eocene-Oligocene transition, *Paleoceanography*, *29*, 810–823, doi:10.1002/2013PA002593.
Lear, C. H., and Y. Rosenthal (2006), Benthic foraminiferal Li/Ca: Insights into Cenozoic seawater carbonate saturation state, *Geology*, *34*(11), 985, doi:10.1130/G22792A.1.
Lear, C. H., Y. Rosenthal, H. K. Coxall, and P. A. Wilson (2004), Late Eocene to early Miocene ice sheet dynamics and the global carbon cycle, *Paleoceanography*, *19*, PA4015, doi:10.1029/2004PA001039.

Lear, C. H., T. R. Bailey, P. N. Pearson, H. K. Coxall, and Y. Rosenthal (2008), Cooling and ice growth across the Eocene-Oligocene transition, *Geology*, *36*(3), 251, doi:10.1130/G24584A.1.
Liu, Z., M. Pagani, D. Zinniker, R. M. DeConto, M. Huber, H. Brinkhuis, S. R. Shah, R. M. Leckie, and A. Pearson (2009), Global cooling during the Eocene-Oligocene climate transition, *Science*, *323*(5918), 1187–1190.
Lyle, M. W. (2003), Neogene carbonate burial in the Pacific Ocean, *Paleoceanography*, *18*(3, 1059), doi:10.1029/2002PA000777.
Lyle, M., J. Barron, T. J. Bralower, M. Huber, A. O. Lyle, A. C. Ravelo, D. K. Rea, and P. A. Wilson (2008), Pacific ocean and Cenozoic evolution of climate, *Rev. Geophys.*, *46*, RG2002, doi:10.1029/2005RG000190.
MacDonald, G. M., D. W. Beilman, K. V. Kremenetski, Y. Sheng, L. C. Smith, and A. A. Velichko (2006), Rapid early development of circumarctic peatlands and atmospheric CH_4 and CO_2 variations, *Science*, *314*(5797), 285–8, doi:10.1126/science.1131722.
Merico, A., T. Tyrrell, and P. A. Wilson (2008), Eocene/Oligocene ocean de-acidification linked to Antarctic glaciation by sea-level fall, *Nature*, *452*(7190), 979–82, doi:10.1038/nature06853.
Miller, K. G., J. V. Browning, M.-P. Aubry, B. S. Wade, M. E. Katz, A. A. Kulpecz, and J. D. Wright (2008), Eocene-Oligocene global climate and sea-level changes: St. Stephens Quarry, Alabama, *Geol. Soc. Am. Bull.*, *120*(1–2), 34–53, doi:10.1130/B26105.1.
Miller, K. G., J. D. Wright, M. E. Katz, B. S. Wade, J. V. Browning, and B. S. Cramer (2009), Climate threshold at the Eocene-Oligocene transition: Antarctic ice sheet influence on ocean circulation, in *SPE452: The Late Eocene Earth—Hothouse, Icehouse, and Impacts*, *Geol. Soc. of Am. Spec. Pap.*, vol. 452, 80301, Geol. Soc. of Am., Boulder, Colo.
Moore, T. C. J. (2013), Erosion and reworking of Pacific sediments near the Eocene-Oligocene boundary, *Paleoceanography*, *28*, 263–273, doi:10.1002/palo.20027.
Mucci, A., and J. W. Morse (1984), The solubility of calcite in seawater solutions of various magnesium concentration, It = 0.697 m at 25 °C and one atmosphere total pressure, *Geochim. Cosmochim. Acta*, *48*, 815–822.
Munhoven, G. (2002), Glacial–interglacial changes of continental weathering: Flux variations estimates of the related CO_2 and HCO_3 and their uncertainties, *Global Planet. Change*, *33*, 155–176.
Oehlert, A. M., K. A. Lamb-Wozniak, Q. B. Devlin, G. J. Mackenzie, J. J. G. Reijmer, and P. K. Swart (2012), The stable carbon isotopic composition of organic material in platform derived sediments: Implications for reconstructing the global carbon cycle, *Sedimentology*, *59*(1), 319–335, doi:10.1111/j.1365-3091.2011.01273.x.
Ogg, J. G., and A. G. Smith (2004), The geomagnetic polarity time scale, in *A Geologic Time Scale*, edited by F. M. Gradstein, J. G. Ogg, and A. G. Smith, pp. 63–86, Cambridge Univ. Press, Cambridge, U. K.
Olivarez Lyle, A., and M. W. Lyle (2006), Missing organic carbon in Eocene marine sediments: Is metabolism the biological feedback that maintains end-member climates?, *Paleoceanography*, *21*, PA2007, doi:10.1029/2005PA001230.
Opdyke, B. N., and B. H. Wilkinson (1988), Surface area control of shallow cratonic to deep marine carbonate accumulation, *Paleoceanography*, *3*(6), 685–703.
Pagani, M., M. Huber, Z. Liu, S. M. Bohaty, J. Henderiks, W. Sijp, S. Krishnan, and R. M. DeConto (2011), The role of carbon dioxide during the onset of Antarctic glaciation, *Science*, *334*(6060), 1261–4, doi:10.1126/science.1203909.
Palike, H., R. D. Norris, J. O. Herrle, P. A. Wilson, H. K. Coxall, C. H. Lear, N. J. Shackleton, A. K. Tripati, and B. S. Wade (2006), The heartbeat of the Oligocene climate system, *Science*, *314*(5807), 1894–1898, doi:10.1126/science.1133822.
Pälike, H., et al. (2012), A Cenozoic record of the equatorial Pacific carbonate compensation depth, *Nature*, *488*(7413), 609–614, doi:10.1038/nature11360.
Pearson, P. N., G. L. Foster, and B. S. Wade (2009), Atmospheric carbon dioxide through the Eocene-Oligocene climate transition, *Nature*, *461*(7267), 1110–3, doi:10.1038/nature08447.
Pekar, S. F., N. Christie-Blick, M. A. Kominz, and K. G. Miller (2002), Calibration between eustatic estimates from backstripping and oxygen isotopic records for the Oligocene, *Geology*, *30*(10), 903, doi:10.1130/0091-7613(2002)030<0903:CBEEFB>2.0.CO;2.
Ravizza, G., and B. Peucker-Ehrenbrink (2003), The marine $^{187}Os/^{188}Os$ record of the Eocene-Oligocene transition: The interplay of weathering and glaciation, *Earth Planet. Sci. Lett.*, *210*(1–2), 151–165, doi:10.1016/S0012-821X(03)00137-7.
Rea, D. K., and M. W. Lyle (2005), Paleogene calcite compensation depth in the eastern subtropical Pacific: Answers and questions, *Paleoceanography*, *20*, PA1012, doi:10.1029/2004PA001064.
Salamy, K. A., and J. C. Zachos (1999), Latest Eocene–early Oligocene climate change and Southern Ocean fertility: Inferences from sediment accumulation and stable isotope data, *Palaeogeogr. Palaeoclimatol. Palaeoecol.*, *145*(1–3), 61–77, doi:10.1016/S0031-0182(98)00093-5.
Scher, H. D., and E. E. Martin (2006), Timing and climatic consequences of the opening of Drake Passage, *Science*, *312*(5772), 428–30, doi:10.1126/science.1120044.
Scher, H. D., S. M. Bohaty, J. C. Zachos, and M. L. Delaney (2011), Two-stepping into the icehouse: East Antarctic weathering during progressive ice-sheet expansion at the Eocene-Oligocene transition, *Geology*, *39*(4), 383–386, doi:10.1130/G31726.1.
Spero, H. J., J. Bijma, D. W. Lea, and B. E. Bemis (1997), Effect of seawater carbonate concentration on foraminiferal carbon and oxygen isotopes, *Nature*, *390*(6659), 497–500, doi:10.1038/37333.
Swart, P. K. (2008), Global synchronous changes in the carbon isotopic composition of carbonate sediments unrelated to changes in the global carbon cycle, *Proc. Natl. Acad. Sci. U.S.A.*, *105*(37), 13,741–13,745, doi:10.1073/pnas.0802841105.
Swart, P. K., and G. Eberli (2005), The nature of the $\delta^{13}C$ of periplatform sediments: Implications for stratigraphy and the global carbon cycle, *Sediment. Geol.*, *175*, 115–129, doi:10.1016/j.sedgeo.2004.12.029.
Swart, P. K., J. J. G. Reijmer, and R. Otto (2009), A re-evaluation of facies on Great Bahama Bank II: Variations in the $\delta^{13}C$, $\delta^{18}O$ and mineralogy of surface sediments, *Int. Assoc. Sedimentol. Spec. Publ.*, *41*, 47–59, doi:10.1002/9781444312065.ch4.
Tarnocai, C., J. G. Canadell, E. A. G. Schuur, P. Kuhry, G. Mazhitova, and S. Zimov (2009), Soil organic carbon pools in the northern circumpolar permafrost region, *Global Biogeochem. Cycles*, *23*, GB2023, doi:10.1029/2008GB003327.
Tigchelaar, M., A. S. Von Der Heydt, and H. A. Dijkstra (2011), A new mechanism for the two-step $\delta^{18}O$ signal at the Eocene-Oligocene boundary, *Clim. Past*, *7*, 235–247, doi:10.5194/cp-7-235-2011.
Tyrrell, T., and R. E. Zeebe (2004), History of carbonate ion concentration over the last 100 million years, *Geochim. Cosmochim. Acta*, *68*(17), 3521–3530, doi:10.1016/j.gca.2004.02.018.
Van de Flierdt, T. (2011), Continental weathering through the onset of Antarctic glaciation, *Geology*, *39*(4), 415–416, doi:10.1130/focus042011.1.
Wade, B. S., A. J. P. Houben, W. Quaijtaal, S. Schouten, Y. Rosenthal, K. G. Miller, M. E. Katz, J. D. Wright, and H. Brinkhuis (2011), Multiproxy record of abrupt sea-surface cooling across the Eocene-Oligocene transition in the Gulf of Mexico, *Geology*, *40*(2), 159–162, doi:10.1130/G32577.1.
Wadham, J. L., et al. (2012), Potential methane reservoirs beneath Antarctica, *Nature*, *488*(7413), 633–7, doi:10.1038/nature11374.
Wallmann, K., E. Pinero, E. Burwicz, M. Haeckel, C. Hensen, A. Dale, and L. Ruepke (2012), The global inventory of methane hydrate in marine sediments: A theoretical approach, *Energies*, *5*(12), 2449–2498, doi:10.3390/en5072449.

Westerhold, T., U. Röhl, H. Pälike, R. Wilkens, P. A. Wilson, and G. Acton (2014), Orbitally tuned timescale and astronomical forcing in the middle Eocene to early Oligocene, *Clim. Past*, *10*(3), 955–973, doi:10.5194/cp-10-955-2014.

Zachos, J. C., and L. R. Kump (2005), Carbon cycle feedbacks and the initiation of Antarctic glaciation in the earliest Oligocene, *Global Planet. Change*, *47*(1), 51–66, doi:10.1016/j.gloplacha.2005.01.001.

Zachos, J. C., T. M. Quinn, and K. A. Salamy (1996), High-resolution (10^4 years) deep-sea foraminiferal stable isotope records of the Eocene-Oligocene climate transition, *Paleoceanography*, *11*(3), 251–266.

Zachos, J. C., B. N. Opdyke, T. M. Quinn, C. E. Jones, and A. N. Halliday (1999), Early Cenozoic glaciation, antarctic weathering, and seawater: Is there a link?, *Chem. Geol.*, *161*(1–3), 165–180, doi:10.1016/S0009-2541(99)00085-6.

Zachos, J. C., M. Pagani, L. Sloan, E. Thomas, and K. Billups (2001), Trends, rhythms, and aberrations in global climate 65 Ma to present, *Science*, *292*(5517), 686–93, doi:10.1126/science.1059412.

Zech, R., Y. Huang, M. Zech, R. Tarozo, and W. Zech (2011), High carbon sequestration in Siberian permafrost loess-paleosols during glacials, *Clim. Past*, *7*(2), 501–509, doi:10.5194/cp-7-501-2011.

Zeng, N. (2003), Glacial-interglacial atmospheric CO_2 change—The glacial burial hypothesis, *Adv. Atmos. Sci.*, *20*(5), 677–693, doi:10.1007/BF02915395.

Zimov, N. S., S. A. Zimov, A. E. Zimova, G. M. Zimova, V. I. Chuprynin, and F. S. Chapin (2009), Carbon storage in permafrost and soils of the mammoth tundra-steppe biome: Role in the global carbon budget, *Geophys. Res. Lett.*, *36*, L02502, doi:10.1029/2008GL036332.